# Study of porous silicon layer effect in optoelectronics properties of crystalline silicon

## Mouna Jemli, Bilel Abdouli, Lotfi Khezami & Mohamed Ben Rabha

Published online: 04 Jun 2023.

Submit your article to this journal ⤤

View related articles ⤤

View Crossmark data ⤤

Taylor & Francis
Taylor & Francis Group

Check for updates

# Study of porous silicon layer effect in optoelectronics properties of crystalline silicon

Mouna Jemli[a], Bilel Abdouli[a], Lotfi Khezami[b], and Mohamed Ben Rabha[a]

[a]Laboratoire de Nanomatériaux et Systèmes Pour Énergies Renouvelables, Centre de Recherches et des Technologies de l'Énergie, Technopôle de Borj-Cédria, Tunis, Tunisie; [b]Chemistry Department, College of Science, Imam Mohammad Ibn Saud Islamic University (IMSIU), Riyadh, Saudi Arabia

**ABSTRACT**

In this research, we experimentally and numerically demonstrate the beneficial effect of superficial porous silicon layer in the optoelectronics properties of multi-crystalline silicon. The hydrogen and oxygen-rich porous silicon layer was formed using vapor etching method. From laser beam induced current (LBIC) simulations, we found that the hydrogen and oxygen-rich porous silicon layer used in mc-Si surface acts as a good surface passivation and a potential candidate for electronic quality and optoelectronics properties improvement. As a result, the generated current of treated silicon is 5 times greater as compared to reference substrate, which led to a 50% increase of the minority carrier diffusion length, 25% decrease in the recombination velocity of the minority carrier and the reflectivity reduced from 38 to 3% of the related sample.
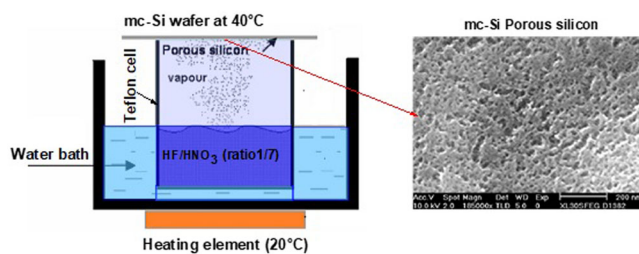
**GRAPHICAL ABSTRACT**



## Introduction

Multicrystalline silicon (mc-Si) is a very attractive material for photovoltaic (PV) cell processing, and mostly used in commercial photovoltaic cell production, due to its low wafer cost compared to crystalline silicon (c-Si).[1] The cell performance of mc-Si is as yet lower than that of monocrystalline (c-Si), due to its intrinsic properties. The mc-Si contains many individual crystals, or grains, that are oriented in different directions. The boundaries between these grains are known as grain boundaries (GBs), and they can act as traps for impurities and defects, which can degrade the performance of the material.

In addition to GBs, mc-Si can also contain stacking faults and dislocations, which are structural defects that can result from the manufacturing process or from handling and processing the material. These defects can also act as traps for impurities and can reduce the efficiency of solar cells made from mc-Si.

Overall, improving the quality of mc-Si by reducing the number and severity of these defects is an ongoing area of research and development in the field of photovoltaics.[2]

The impurity–defect interactions decrease the optoelectronics properties of multi-crystalline silicon, such as the lifetime of minority charge carriers in the as-cut wafer compared to their c-Si counterpart. To overcome these problems, there are several ways to improve the optoelectronic properties of multicrystalline silicon[3]; doping mc-Si with impurities such as boron or phosphorus can increase electron mobility and reduce defect density, thus improving its optoelectronic properties, applying an antireflective coating to the surface of mc-Si can reduce reflectance and increase light absorption[4–6]. These techniques have been shown to effectively improve the optoelectronic properties of mc-Si and increase the efficiency of photovoltaic cells made from this material. The optoelectronics properties of multi-crystalline silicon can be improved by oxygen and hydrogen passivation of crystal defects of mc-Si,[7–9] can reduce surface recombination of electrons and holes, increasing the efficiency of the photovoltaic cells.

Recently, many authors have attempted to introduce oxygen and hydrogen in order to passivate c-Si or mc-Si wafers directly by exposing Si wafers to $HNO_3/HF$ vapor
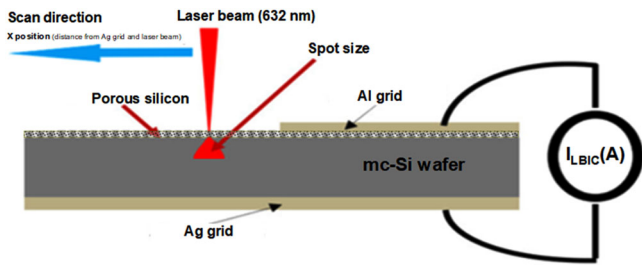
**Figure 1.** Experimental set-up for LBIC technique.

etching.[10,11] The objective of this investigation is to show the effectiveness of oxygen and hydrogen-rich porous silicon on the surface passivation and electronic property enhancement of multi-crystalline silicon. A discussion of the effect of oxygen and hydrogen- rich porous silicon on the optoelectronic quality of mc-Si is presented.

In the context of optoelectronics, the microstructure of the multicrystalline silicon, the reflectivity of mc-Si surface, the quality of the passivating layer and the Light Beam Induced Current LBIC measurements were performed to
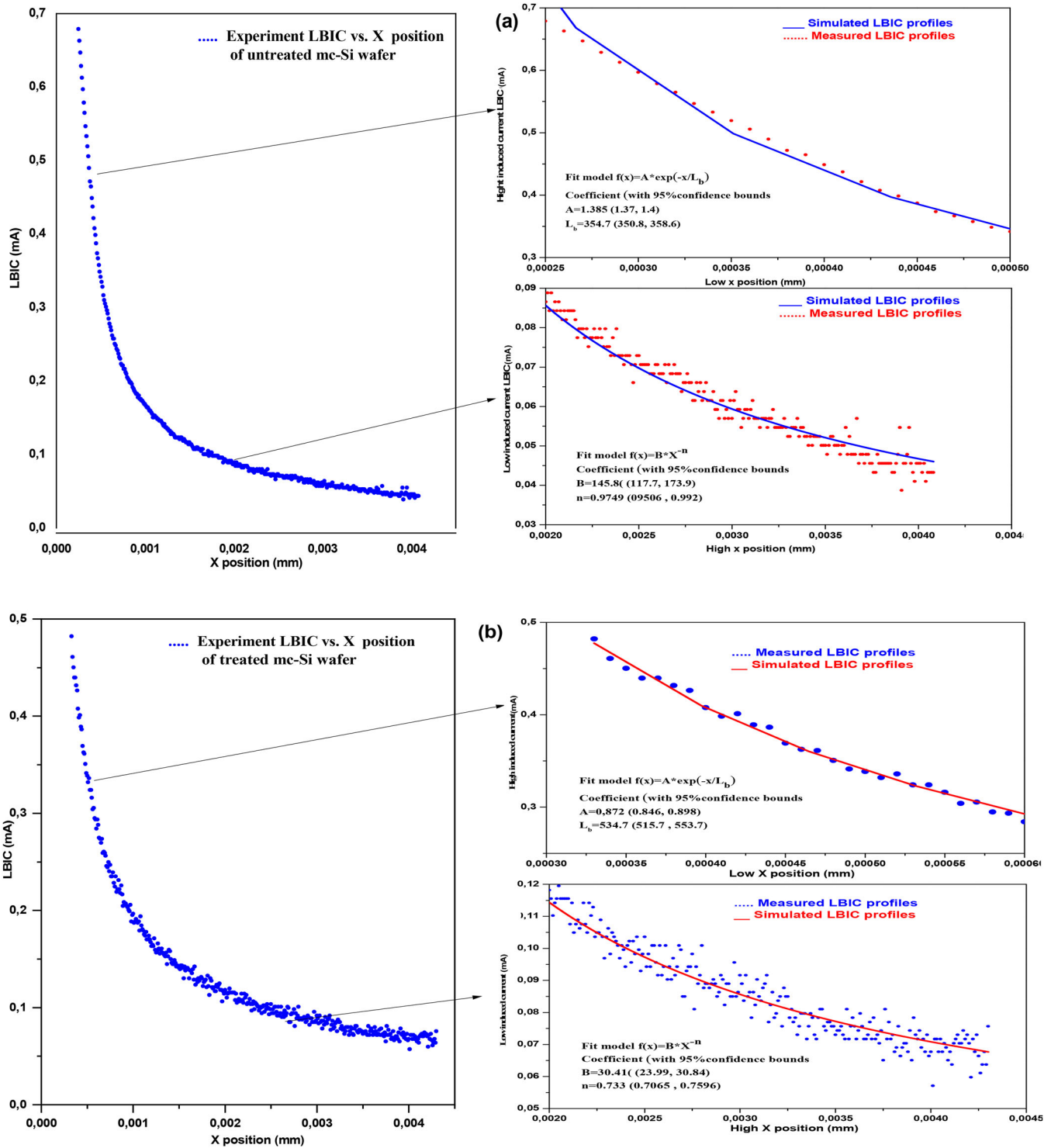


**Figure 2.** LBIC profiles for (a) untreated mc-Si, (b) vapor etching -treated mc-Si. Full lines correspond to theoretical simulation.

**Table 1.** Diffusion Length $L_b$ estimates for untreated and treated samples.

| Fit Model $f(x) = A*\exp(-x/L)$ | $A$ | 95% confidence bounds | $L_b$ (μm) | 95% confidence bounds | $R^2$ |
|---|---|---|---|---|---|
| Untreated | 1.385 | (1.37, 1.4) | 354.7 | (350.8, 358.6) | 0.9924 |
| Treated | 0.872 | (0.846, 0.898) | 534.7 | (515.7, 553.7) | 0.9994 |

**Table 2.** Exponent ($n$) estimates for untreated and treated samples.

| Fit Model $f(x) = B*x^{-n}$ | $B$ | 95% confidence bounds | $n$ | 95% confidence bounds | $R^2$ |
|---|---|---|---|---|---|
| Untreated | 145.8 | (117.7, 173.9) | 0.9749 | (0.9506, 0.9992) | 0.9747 |
| Treated | 30.41 | (23.99, 30.84) | 0.733 | (0.7065, 0.7596) | 0.931 |
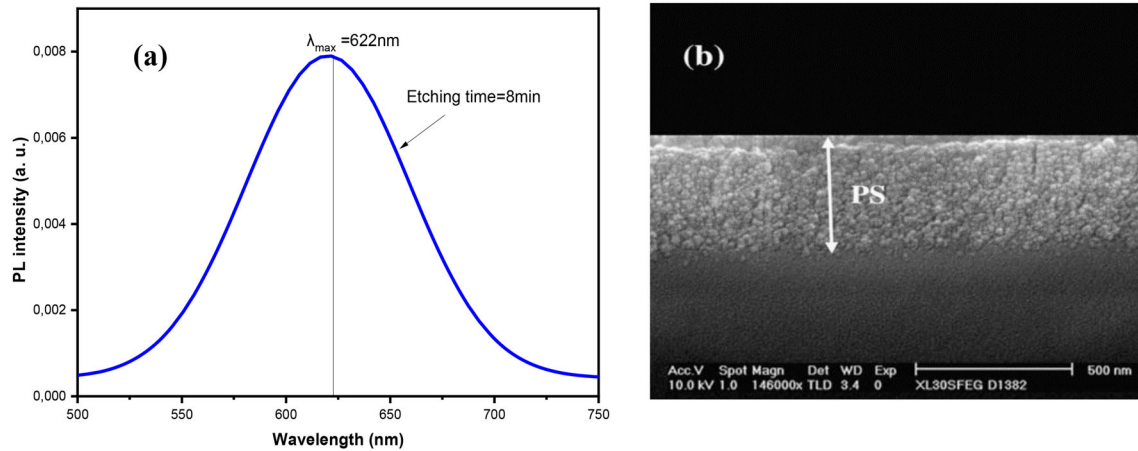


**Figure 3.** (a)Photoluminescence and (b) cross section of Scanning Electron images of the fabricated porous silicon layer.
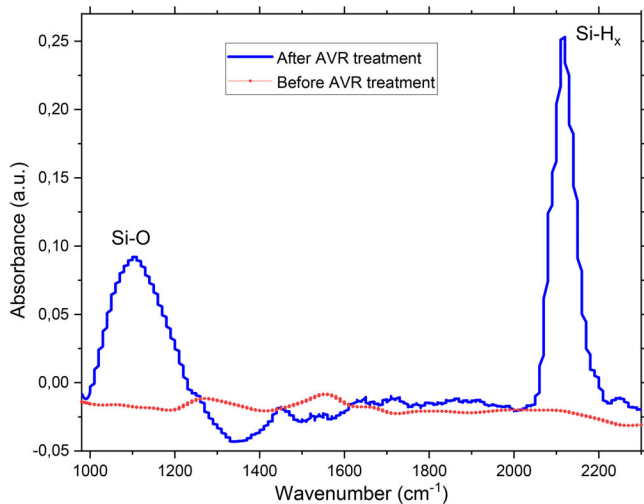


**Figure 4.** FTIR spectra before and after porous silicon formation.

characterize the passivation effect of oxygen and hydrogen-rich porous silicon.

## Results and discussion

In the context of optoelectronics, LBIC, FTIR, SEM and reflectivity can be used to determine the quality of the passivating layers used in mc-Si wafer. To examine the passivation effect by the hydrogen and oxygen-rich porous silicon layer used in mc-Si wafer we need to quantify the electronic quality of the wafer before and after vapor etching. For this purpose, LBIC current was measured by scanning the mc-Si wafer by He–Ne 632 nm wavelength of approximately 150 μm spot size shown in Figure 1. The effective diffusion length ($L_b$) and the exponentiation (n) reflecting the surface recombination velocity (Sf) were determined by fitting the experimental LBIC measurements to theoretical models at two regions: (i) at low X-positions, and (ii) far from the collector edge (at high X-positions). Many works dealing with the LBIC technique report using the mathematical model below.[12,13]

$$I_{LBIC}(x) = A*\exp(-x/L_b) \qquad (1)$$

$$I_{LBIC}(x) = B*x^{-n} \qquad (2)$$

where $x$ is the distance from the Ag grid and the laser beam, A and B are constants depending primarily on the beam intensity and the penetration depth, n is a constant depending on the surface recombination velocity and $L_b$ the effective diffusion length.

For thin samples, ($W < 4L_b$) is applicable near the collector edge.[14] Indeed, most often, LBIC measurements are more reliable near the collector edge; consequently, and as a rule of thumb, data corresponding to low X-positions are used to estimate the diffusion length (by Equation 1). On the other hand, at high X-positions a power law (Equation 2) predominates and from which we can estimate the exponentiation parameter (n) which reflects the surface recombination velocity

Fitting results using MATLAB Curve-Fitting Toolbox are summarized in Tables 1 and 2. Measured and simulated LBIC profiles associated to mc-Si before and after vapor etching are presented in Figure 2.
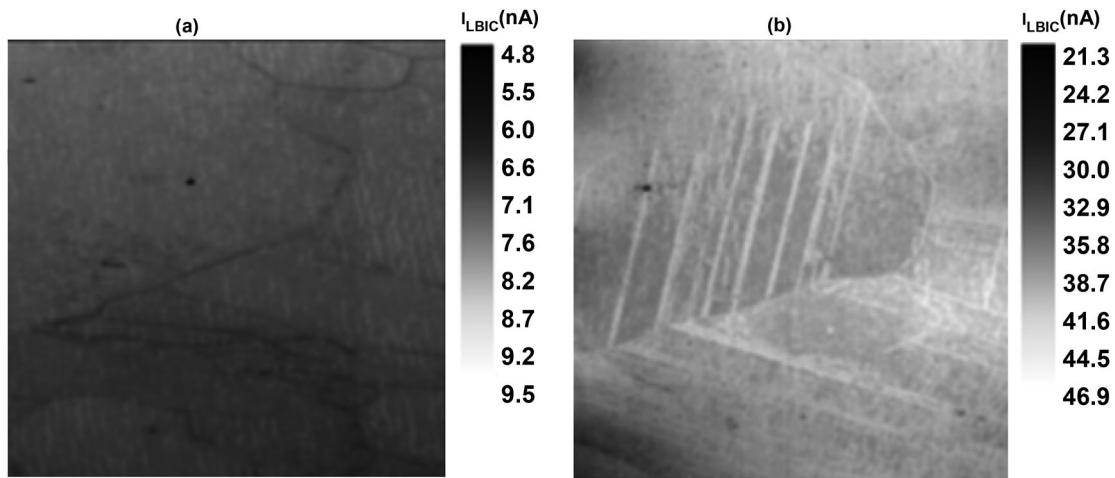
**Figure 5.** Two-dimensional generated current $I_{LBIC}$ (nA) distribution taken from the same region of mc-Si wafer of area $4 \times 2\,\text{mm}^2$ (a) before and (b) after porous silicon formation by vapor etching method.
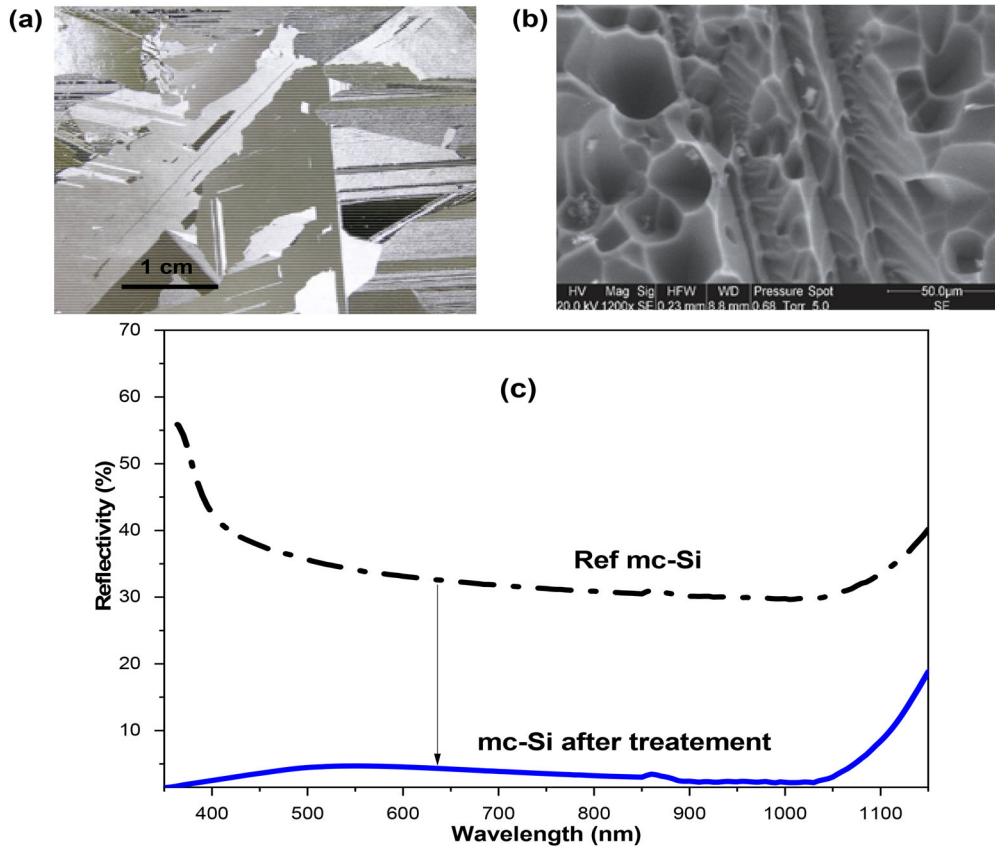


**Figure 6.** SEM images (a) for ref mc-Si and (b) after vapor etching treatment support the decrease in the reflectivity, (c) total reflectivity of mc-Si surface before and after vapor etching treatment.

The photoluminescence spectra and the cross section of Scanning Electron images of the fabricated porous silicon layer are shown in Figure 3. We observed that the produced porous silicon layer result in an emission band over the visible light region and have an emission peak centered at 622 nm. The energy gap ($E_g$) of PS layers is determined by:

$$E_g = \frac{hc}{\lambda_{Max}} \tag{3}$$

where $h$ is the Planck's constant, $c$ is the speed of light and $\lambda_{max}$ is the wavelength corresponding to the peak of PL spectra. The calculated energy bandgap of the porous silicon layers (1.99 eV) is higher than the (1.12 eV) corresponding to silicon single crystal bandgap energy value,[15] which is attributed to the formation of porous layer with small pore size.[16]

FTIR can be used to study the chemical composition of the porous silicon, and to determine the quality of the used passivating layer. As shown in Figure 4, two major bands correspond to samples following vapor etching treatment; the first band is located at 1022–1159 cm$^{-1}$ and the second is around 2048–2258 cm$^{-1}$. The second bonds are ascribed
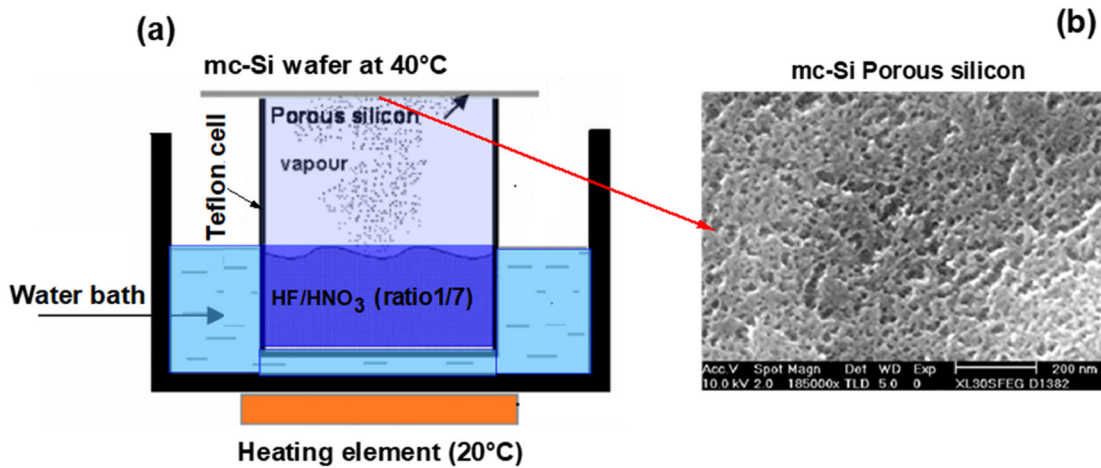
**Figure 7.** (a) Experimental set-up for the vapor etching technique and (b) SEM images of mc-Si porous silicon.

to Si-H stretching modes of the form Si-Hx, and $x = 1$, 2 and 3, respectively. The primary band is associated to oxygen, typically Si–O stretching in O–Si–O and c-Si–O.[17] Considering the above observation, it appears from the FTIR spectra that samples having higher concentrations of O and H in both bands specific to hydrogen and oxygen-rich porous silicon. This confirmed that the diffusion length $L_b$ depends both on hydrogen and oxygen passivation of the silicon wafers which plays a fundamental role in decreasing the non-radiative Si dangling bond defects. As a consequence, this leads to an increase of the diffusion length $L_b$ from about 355 to 535 μm and decrease in the exponentiation (n) from 0.97 to 0.73 (25% decrease) following vapor etching treatment. These results indicate high electronic quality and an improvement of the optoelectronics properties of multi-crystalline silicon wafer.[3,18]

Two-dimensional generated current (GC) $I_{LBIC}$ method[19] was performed on the same region mc-Si sample of an area $4 \times 2 \, mm^2$ before and after porous silicon treatment. A significant variation in the produced current was observed after porous silicon treatment, as a result of variations in the defects density. After vapor etching, current mapping analysis illustrates an enhancement of the $I_{LBIC}$ compared to mc-Si before vapor etching. The GC changes between 4.98 and 9.52 nA (Figure 5a). However, after vapor etching treatment (Figure 5b) the lowest GC value becomes 21.3 nA and the extreme value reaches 46.9 nA. This progression in the GC can be explained by an enhancement of both the minority carrier diffusion length and the recombination centers passivation at the grains and GBs as matched to the reference substrate.

The $I_{LBIC}$ map of untreated mc-Si sample shows a tangle of dark lines that correspond to regions with high carrier capture rates, owed to GBs related defects, which represents the grain boundaries (GBs). Furthermore, the $I_{LBIC}$ signal shows other large areas less dark than GBs which represents the grain of mc-Si (Figure 5a). After vapor etching (Figure 5b) we observe the disappearance of the dark areas in both grain and grain boundaries of mc-Si. Therefore, this disappearance can be ascribed to the diminution of defects density as a consequence of hydrogen and oxygen

passivation effect.[20–24] This plays a key role for an excellent surface passivation and high electronic quality of multi-crystalline silicon; as a result, the generated current improved from 9.5 nA for untreated mc-Si to ∼ 47 nA after vapor etching treatment at the current maximum measured points. Further, important reflectivity reduction was observed after vapor etching (Figure 6c), due to the change on the mc-Si surface morphology and comparable to silicon nanowire's structure,[20] where the SEM images showed in Figure 6a and b before and after vapor etching treatment support this decrease in the reflectivity. As a consequence, this leads to a reduction from 38 to 3% of the treated sample. Thus, the diminution of the reflectivity (augmentation of absorption) is found to be accompanied by a rise of the minority carrier diffusion length.[24]

## Experimental

Industrial p-type mc-Si Czochralskyc (CZ)-grown crystalline silicon wafers with resistivity 0.5–2 Ω.cm and thickness 330 μm were used in this work. Oxygen and Hydrogen-rich porous silicon was achieved by vapor etching technique, which consists of exposing the mc-Si substrates to acid vapor issued from a mixture acid of $HNO_3$ (65%)/HF (40%).

In this experiment, to achieve porous silicon the $HNO_3$/HF volume ratio were fixed to 1/7 and the etching time was optimized to 8 min, while the temperatures of the acid solution and the silicon substrate were fixed to 20 and 40 °C, respectively. This modification in temperature is necessary to evade vapor condensation on the silicon surface during vapor etching process (Figure 7a, b) shows the experimental set-up for the vapor etching technique and SEM images of mc-Si nanostructures obtained after vapor etching.

## Conclusions

In this article, we demonstrated that the sensing oxygen and hydrogen-rich porous silicon layer produced by vapor etching method provide higher electronic quality multi-crystalline silicon. The hydrogen and oxygen- rich porous silicon layer formed in mc-Si surface acts as a good surface

passivation and a potential candidate for electronic and optoelectronics properties improvement. As a result, the generated current of treated silicon is 21 times greater as compared to reference substrate, which led to a 50% increase of the minority carrier diffusion length and 25% decrease in the recombination velocity of the minority carrier. Reflectivity reduction from 38 to 3% was observed after PS formation. These results are of universal importance both in passivation and electronic quality improvement of mc-Si, that make them a good option for the advancement of efficiency in a photovoltaic cell.

## Acknowledgments

## Disclosure Statement

The authors declare no conflict of interest.

## ORCID

Mohamed Ben Rabha http://orcid.org/0000-0001-7118-8635

## References

[1] Ballif, C.; Haug, F. J.; Boccard, M.; Verlinden, P. J.; Hahn, G. Status and Perspectives of Crystalline Silicon Photovoltaics in Research and Industry. *Nat. Rev. Mater.* **2022**, *7*, 597–616. DOI: 10.1038/s41578-022-00423-2.

[2] Rabha, M. B.; Khezami, L.; Jemai, A. B.; Alhathlool, R.; Ajbar, A. Surface Passivation of Silicon Nanowires Based Metal Nano-Particle Assisted Chemical Etching for Photovoltaic Applications. *J. Cryst. Growth* **2017**, *462*, 35–40. DOI: 10.1016/j.jcrysgro.2017.01.021.

[3] Khezami, L.; Jemai, A. B.; Alhathlool, R.; Rabha, M. B. Electronic Quality Improvement of Crystalline Silicon by Stain Etching-Based PS Nanostructures for Solar Cells Application. *Sol. Energy* **2016**, *129*, 38–44. DOI: 10.1016/j.solener.2016.01.034.

[4] Muduli, S. P.; Kale, P. State-of-the-Art Passivation Strategies of c-Si for Photovoltaic Applications: A Review. *Mater. Sci. Semicond. Process* **2023**, *154*, 107202. DOI: 10.1016/j.mssp.2022.107202.

[5] Lingaraja, D.; Kumar, S. P.; Ram, G. D.; Ramya, S. Experimental Investigation of Influence of Electrolytic Solution in Porous Silicon Formation for Solar Energy Conversion. *Silicon* **2023**, *15*, 1–8. DOI: 10.1007/s12633-023-02305-w.

[6] Zhou, J.; Su, X.; Huang, Q.; Zhang, B.; Yang, J.; Zhao, Y.; Hou, G. Recent Advancements in Poly-Si/SiOx Passivating Contacts for High-Efficiency Silicon Solar Cells: Technology Review and Perspectives. *J. Mater. Chem. A* **2022**, *10*, 20147–20173. DOI: 10.1039/D2TA04730F.

[7] Strehlke, S.; Bastide, S.; Lévy-Clément, C. Optimization of Porous Silicon Reflectance for Silicon Photovoltaic Cells. *Sol. Energy Mater. Sol. Cel.* **1999**, *58*, 399–409. DOI: 10.1016/S0927-0248(99)00016-1.

[8] Bilyalov, R. R.; Lüdemann, R.; Wettling, W.; Stalmans, L.; Poortmans, J.; Nijs, J.; Schirone, L.; Sotgiu, G.; Strehlke, S.; Lévy-Clément, C.; et al. Multicrystalline Silicon Solar Cells with Porous Silicon Emitter. *Sol. Energy Mater. Sol. Cel.* **2000**, *60*, 391–420. DOI: 10.1016/S0927-0248(99)00102-6.

[9] Saadoun, M.; Mliki, N.; Kaabi, H.; Daoudi, K.; Bessaïs, B.; Ezzaouia, H.; Bennaceur, R. Vapour-Etching-Based Porous

[10] Silicon: A New Approach. *Thin Solid Films* **2002**, *405*, 29–34. DOI: 10.1016/S0040-6090(01)01757-6.

[10] Ben Jaballah, A.; Hassen, M.; Hajji, M.; Saadoun, M.; Bessais, B.; Ezzaouia, H. Chemical Vapour Etching of Silicon and Porous Silicon: Silicon Solar Cells and Micromachining Applications. *Phys. Stat. Sol. (a)* **2005**, *202*, 1606–1610. DOI: 10.1002/pssa.200461197.

[11] Davidson, S. M.; Dimitriadis, C. A. Advances in the Electrical Assessment of Semiconductors Using the Scanning Electron Microscope. *J. Microsc.* **1980**, *118*, 275–290. DOI: 10.1111/j.1365-2818.

[12] Sayad, Y.; Kaminski, A.; Blanc, D.; Nouiri, A.; Lemiti, M. Determination of Diffusion Length in Photovoltaic Crystalline Silicon by Modelisation of Light Beam Induced Current. *Superlattices Microstruct.* **2009**, *45*, 393–401. DOI: 10.1016/j.spmi.2008.11.002.

[13] Sayaad, Y. Détermination de la longueur de diffusion des porteurs minoritaires dans le silicium cristallin par interaction lumière-matière. Ph.D. INSA, Lyon, French, **2009**.

[14] Bisi, O.; Ossicini, S.; Pavesi, L. Porous Silicon: A Quantum Sponge Structure for Silicon Based Optoelectronics. *Surf. Sci. Rep.* **2000**, *38*, 1–126. DOI: 10.1016/S0167-5729(99)00012-6.

[15] Youssef, G. M.; El-Nahass, M. M.; El-Zaiat, S. Y.; Farag, M. A. Investigation of Size and Band Gap Distributions of Si Nanoparticles from Morphology and Optical Properties of Porous Silicon Layers Formed on a Textured N + P Silicon Solar Cell. *Int. J. Semicond. Sci. Technol.* **2016**, *6*, 1–12. DOI: IJSSTFEB20161.

[16] Butturi, M. A.; Carotta, M. C.; Martinelli, G.; Passari, L.; Youssef, G. M.; Chiorino, A.; Ghiotti, G. Effects of Ageing on Porous Silicon Photoluminescence: Correlation with FTIR and UV-Vis Spectra. *Solid State Commun.* **1997**, *101*, 11–16. DOI: 10.1016/S0038-1098(96)00539-X.

[17] Ben Rabha, M.; Mohamed, S. B.; Dimassi, W.; Gaidi, M.; Ezzaouia, H.; Bessais, B. Optoelectronic Enhancement of Monocrystalline Silicon Solar Cells by Porous Silicon-Assisted Mechanical Grooving. *Phys. Status Solidi (c)* **2011**, *8*, 887–890. DOI: 10.1002/pssc.201000250.

[18] Dimassi, W.; Derbali, L.; Bouaïcha, M.; Bessaïs, B.; Ezzaouia, H. Two-Dimensional LBIC and Internal-Quantum-Efficiency Investigations of Grooved Grain Boundaries in Multicrystalline Silicon Solar Cells. *Sol. Energy* **2011**, *85*, 350–355. DOI: 10.1016/j.solener.2010.11.014.

[19] Khedher, N.; Hajji, M.; Hassen, M.; Ben Jaballah, A.; Ouertani, B.; Ezzaouia, H.; Bessais, B.; Selmi, A.; Bennaceur, R. Gettering Impurities from Crystalline Silicon by Phosphorus Diffusion Using a Porous Silicon Layer. *Sol. Energy Mater. Sol. Cell* **2005**, *87*, 605–611. DOI: 10.1016/j.solmat.2004.09.017.

[20] Nafie, N.; Lachiheb, M. A.; Rabha, M. B.; Dimassi, W.; Bouaïcha, M. Effect of the Doping Concentration on the Properties of Silicon Nanowires. *Phys. E: Low-Dimens. Syst. Nanostruct.* **2014**, *56*, 427–430. DOI: 10.1016/j.physe.2012.10.007.

[21] Einhaus, R.; Duerinckx, F.; Van Kerschaver, E.; Szlufcik, J.; Durand, F.; Ribeyron, P. J.; Duby, J. C.; Sarti, D.; Goaer, G.; Le, G. N.; et al. Hydrogen Passivation of Newly Developed EMC-Multi-Crystalline Silicon. *Mater. Sci. Eng. B* **1999**, *58*, 81–85. DOI: 10.1016/S0921-5107(98)00286-4.

[22] Khezami, L.; Al Megbel, A. O.; Jemai, A. B.; Rabha, M. B. Theoretical and Experimental Analysis on Effect of Porous Silicon Surface Treatment in Multicrystalline Silicon Solar Cells. *Appl. Surf. Sci.* **2015**, *353*, 106–111. DOI: 10.1016/j.apsusc.2015.06.090.

[23] Krotkus, A.; Grigoras, K.; Pačebutas, V.; Barsony, I.; Vazsonyi, E.; Fried, M.; Levy-Clement, C. Efficiency Improvement by Porous Silicon Coating of Multicrystalline Solar Cells. *Sol. Energy Mater. Sol. Cell* **1997**, *45*, 267–273. DOI: 10.1016/S0927-0248(96)00073-6.

[24] Hallam, B.; Chan, C.; Abbott, M.; Wenham, S. Hydrogen Passivation of Defect-Rich n-Type Czochralski Silicon and Oxygen Precipitates. *Sol. Energy Mater. Sol. Cell* **2015**, *141*, 125–131. DOI: 10.1016/j.solmat.2015.05.009.